A New Technique for the Skewing Consideration in the 2-D FEM Un-Skewed Induction Motor Time-Dependant Electromagnetic Characteristics

Gyftakis, K. and Kappatou, J. C.

Original citation & hyperlink:
Gyftakis, K. and Kappatou, J. C. (2016) 'A New Technique for the Skewing Consideration in the 2-D FEM Un-Skewed Induction Motor Time-Dependant Electromagnetic Characteristics' In: ICEMS 2016, 'International Conference on Electrical Machines and Systems'. Held 13-16 November 2016 at Chiba, Japan. IEEE
http://ieeexplore.ieee.org/document/7837406/

ISBN 978-4-88686-098-9
ISBN 978-1-4673-8863-4

Publisher: IEEE

A New Technique for the Skewing Consideration in the 2-D FEM Un-Skewed Induction Motor Time-Dependant Electromagnetic Characteristics

Konstantinos N. Gyftakis*, *Member, IEEE* and Joya C. Kappatou**, *Member, IEEE*
* Coventry University, EC Building, Gulson Road, Coventry, CV12JH, UK
** University of Patras, Electrical and Computer Engineering Dept., Rion, 26500, Greece

***Abstract*— The skewing is the most commonly used technique for noise minimization in induction motors. In order to take the skewing into consideration in FEM simulations, one should design a multi-slice 2D model or a 3D model, since the skewing affects the motor design along the shaft axis. As a consequence, the complexity of the FE model increases as well as the computational time, especially when the analysis performed, takes into consideration the non-linearity of the iron core. This paper offers a technique for the skewing consideration in the induction motor, when simulated as un-skewed in transient electromagnetic 2D FEM analysis. The proposed technique could be particularly useful for faster simulations when the necessary simulation time is long, e.g. for diagnostic purposes. Experimental testing verifies the simulations' results with accuracy.**

***Index Terms*— Finite Element Method, Induction Motor, Skewing, Transient Analysis.**

I. Introduction

THE skewing of the cage bars in the induction machine is a rather old technique [1]. It serves for the electromagnetic variables' harmonic content minimization in squirrel-cage induction motors. As a technique, it is also frequent in other types of electrical machines [2]-[5]. During the years, extensive studies have studied skewed induction motors and their characteristics, offering a rich information library on this scientific subject [6]-[9]. Much work has also been accomplished, connecting the skewing with the inter-bar currents and the iron core saturation in induction machines [10]-[12].

Nowadays, a great deal of work, in the scientific research area of electric motors, is performed with Finite Element Analysis. With the use of FEM, researchers are able to take into account the actual geometry and materials' characteristics of the motor. Using FEM one can study also, the spatial and time-dependant electromagnetic characteristics of the electric motor. In order to simulate the skewing, two types of models have been developed and studied so far: the 2-D multi-slice and the 3-D models [13]-[18]. Skewed machines can be modeled as 2-D multi-slice models, using a set of slices which rotate at different angles. Any section of a machine can have a skewing angle. The analysis makes a copy of the mesh for each slice, offsetting all but the central slice by the appropriate angle [19]. Moreover, in each slice a 2-D magnetic field problem is assumed, only the component of the current density perpendicular to the cross-section and that of the perpendicular to the shaft are considered. So in this way the inter-bar currents and the axial saturation variation are neglected [20].

However, the main disadvantage of the FE Analysis still remains and concerns the large computational time [10], especially when the non-linear magnetic characteristics of the rotor and stator iron cores are taken into consideration. Consequently, researchers often simulate the induction motors un-skewed, saving computational time, on the cost of the accuracy.

In this work, a new technique will be presented aiming to aid to in this direction. More specifically, this paper shows how to take into consideration the rotor skewing in the post-processing calculations, while having simulated un-skewed induction motors with 2-D FEM. The proposed technique concerns the time-dependant variables, results of the FE Analysis, such as the stator currents and the electromagnetic torque. So, the proposed technique is particularly useful when the simulation is highly time-consuming e.g. for diagnostic applications using frequency spectrums of the diagnostic means such as currents, torque, power etc [21]-[24].

II. Theoretical Investigation

A. Analytical Calculations for Un-skewed Motor

In this section, the formula which describes the air-gap magnetic flux density of an un-skewed induction motor will be shown. When q is an integer, then the stator's MMF presents space harmonics of rank ν where:

$$\nu = 6\kappa \pm 1 \tag{1}$$

and so, the stator MMF can be written as:

$$F_1(a,t) = \sum_{\nu=6\kappa\pm1}^{\infty} F_{m\nu} \cos\left(\nu p\alpha \mp \omega t\right) \tag{2}$$

Also, for the rotor MMF there is:

$$F_2(a,t)=\sum_{\mu=1}^{\infty}F_{m\mu}\cos(\mu p\alpha\mp\omega t-\varphi) \tag{3}$$

where:

$$\mu=\kappa\frac{s_2}{p}\pm1 \tag{4}$$

and α is the geometrical angle:

$$a=\frac{1}{p}\frac{\pi}{\tau}x \tag{5}$$

According to [25] the air-gap relative permeance is given by:

$$\Lambda_g(\alpha)=\Lambda_{g0}\lambda_{g1}(\alpha)\lambda_{g2}(\alpha) \tag{6}$$

where:

$$\Lambda_{g0}=\frac{\mu_0}{k_c g}=\frac{\mu_0}{g'} \tag{7}$$

$$\lambda_{g1}(\alpha)=1+\sum_{k=1,2,3}^{\infty}\mathrm{A}_k\cos(ks_1\alpha) \tag{8}$$

$$\lambda_{g2}(\alpha)=1+\sum_{l=1,2,3}^{\infty}\mathrm{A}_l\cos\left[ls_2(\alpha-\omega_2 t)\right] \tag{9}$$

and

$$\omega_2=2\pi(1-s)f=2\pi(1-s)n_s p=2\pi n_m p=p\Omega_m \tag{10}$$

A_k and A_l are related to the stator and rotor slot geometrical variables.

So if we introduce (7), (8) and (9) into (6) then:

$$\Lambda_g(\alpha,t)=\Lambda_{g0}\lambda_g(\alpha,t)=\frac{\mu_0}{k_C g}\lambda_g(\alpha,t) \tag{11}$$

where:

$$\begin{aligned}\lambda_g(\alpha,t)=1&+\sum_{k=1,2,3}^{\infty}\mathrm{A}_k\cos(ks_1\alpha)+\sum_{l=1,2,3}^{\infty}\mathrm{A}_l\cos\left[ls_2(\alpha-\omega_2 t)\right]+\\&+\frac{1}{2}\sum_{k=1,2,3}^{\infty}\sum_{l=1,2,3}^{\infty}\mathrm{A}_k\mathrm{A}_l\begin{Bmatrix}\cos\left[(ls_2+ks_1)\alpha-ls_2\omega_2 t\right]+\\\cos\left[(ls_2-ks_1)\alpha-ls_2\omega_2 t\right]\end{Bmatrix}\end{aligned} \tag{12}$$

The first term of (12) describes the equivalent uniform air-gap's permeance, the second and third term describe harmonics of the stator and rotor permeance respectively and the last term represents harmonics of the permeance due to reciprocal effect of the stator and rotor.

The radial component of the air-gap magnetic flux density can be calculated by:

$$b(\alpha,t)=\left[F_1(\alpha,t)+F_2(\alpha,t)\right]\Lambda_g(\alpha,t) \tag{13}$$

Or, if b(α,t) is divided into the stator and rotor MMF contribution to the magnetic flux density :

$$b(\alpha,t)=b_1(\alpha,t)+b_2(\alpha,t) \tag{14}$$

where:

$$b_1(\alpha,t)=F_1(\alpha,t)\Lambda_g(\alpha,t) \tag{15}$$

and

$$b_2(\alpha,t)=F_2(\alpha,t)\Lambda_g(\alpha,t) \tag{16}$$

In order to examine each term of (12), $b_1(\alpha,t)$ is divided into four components:

$$b_1(\alpha,t)=b_1^1(\alpha,t)+b_1^2(\alpha,t)+b_1^3(\alpha,t)+b_1^4(\alpha,t) \tag{17}$$

and each individual term of (17) is:

$$b_1^1(\alpha,t)=\frac{\mu_0}{k_C g}\left[\sum_{\nu=6\kappa\pm1}^{\infty}F_{m\nu}\cos(\nu p\alpha\mp\omega t)\right] \tag{18}$$

$$b_1^2(\alpha,t)=\frac{1}{2}\frac{\mu_0}{k_C g}\sum_{\nu=6\kappa\pm1}^{\infty}\sum_{k=1,2,3}^{\infty}F_{m\nu}\mathrm{A}_k\times\begin{Bmatrix}\cos\left[(\nu p+ks_1)\alpha\mp\omega t\right]+\\\cos\left[(\nu p-ks_1)\alpha\mp\omega t\right]\end{Bmatrix} \tag{19}$$

$$b_1^3=\frac{1}{2}\frac{\mu_0}{k_C g}\sum_{\nu=6\kappa\pm1}^{\infty}\sum_{l=1,2,3}^{\infty}F_{m\nu}\mathrm{A}_l\times\begin{Bmatrix}\cos\left[(\nu p+ls_2)\alpha-(ls_2\omega_2\pm\omega)t\right]+\\\cos\left[(\nu p-ls_2)\alpha+(ls_2\omega_2\mp\omega)t\right]\end{Bmatrix} \tag{20}$$

$$b_1^4=\frac{1}{4}\frac{\mu_0}{k_C g}\sum_{\nu=6\kappa\pm1}^{\infty}\sum_{k=1,2,3}^{\infty}\sum_{l=1,2,3}^{\infty}F_{m\nu}\mathrm{A}_k\mathrm{A}_l\times\begin{Bmatrix}\cos\left[(\nu p+ls_2+ks_1)\alpha-(ls_2\omega_2\pm\omega)t\right]+\\\cos\left[(\nu p-ls_2-ks_1)\alpha+(ls_2\omega_2\mp\omega)t\right]+\\\cos\left[(\nu p+ls_2-ks_1)\alpha-(ls_2\omega_2\pm\omega)t\right]+\\\cos\left[(\nu p-ls_2+ks_1)\alpha+(ls_2\omega_2\mp\omega)t\right]\end{Bmatrix} \tag{21}$$

same for the rotor MMF contribution to the magnetic flux density term:

$$b_2(\alpha,t)=b_2^1(\alpha,t)+b_2^2(\alpha,t)+b_2^3(\alpha,t)+b_2^4(\alpha,t) \tag{22}$$

and each individual term of (22) is:

$$b_2^1(\alpha,t)=\frac{\mu_0}{k_C g}\left[\sum_{\mu=1}^{\infty}F_{m\mu}\cos(\mu p\alpha\mp\omega t-\varphi)\right] \tag{23}$$

$$b_2^2=\frac{1}{2}\frac{\mu_0}{k_C g}\sum_{\mu=1}^{\infty}\sum_{k=1,2,3}^{\infty}F_{m\mu}\mathrm{A}_k\times\begin{Bmatrix}\cos\left[(\mu p+ks_1)\alpha\mp\omega t-\varphi\right]+\\\cos\left[(\mu p-ks_1)\alpha\mp\omega t-\varphi\right]\end{Bmatrix} \tag{24}$$

$$b_2^3=\frac{1}{2}\frac{\mu_0}{k_C g}\sum_{\mu=1}^{\infty}\sum_{l=1,2,3}^{\infty}F_{m\mu}\mathrm{A}_l\times\begin{Bmatrix}\cos\left[(\mu p+ls_2)\alpha-(ls_2\omega_2\pm\omega)t-\varphi\right]+\\\cos\left[(\mu p-ls_2)\alpha+(ls_2\omega_2\mp\omega)t-\varphi\right]\end{Bmatrix} \tag{25}$$

$$b_2^4=\frac{1}{4}\frac{\mu_0}{k_C g}\sum_{\mu=1}^{\infty}\sum_{k=1,2,3}^{\infty}\sum_{l=1,2,3}^{\infty}F_{m\mu}\mathrm{A}_k\mathrm{A}_l\times\begin{Bmatrix}\cos\left[\mu p\alpha\mp\omega t-\varphi+(ls_2+ks_1)\alpha-ls_2\omega_2 t\right]+\\\cos\left[\mu p\alpha\mp\omega t-\varphi-(ls_2+ks_1)\alpha+ls_2\omega_2 t\right]+\\\cos\left[\mu p\alpha\mp\omega t-\varphi+(ls_2-ks_1)\alpha-ls_2\omega_2 t\right]+\\\cos\left[\mu p\alpha\mp\omega t-\varphi+(ls_2-ks_1)\alpha+ls_2\omega_2 t\right]\end{Bmatrix} \tag{26}$$

In equations (20), (21), (25) and (26), one can observe the existence of the rotor slot related harmonics $ls_2\omega_2 t$. They depend on the rotor slot number and the mechanical angular velocity, consequently also dependant on the operating slip.

Also, there are spatial rotor slot related harmonics in equations (23)-(26): $\mu p\alpha$, $(\mu p+ls_2)\alpha$, which depend on the geometrical angle, the rotor slot number and the number of pole pairs. The skewing is implemented in the induction motors aiming to significantly decrease the amplitudes of the above slot harmonics.

According to [25], the air-gap relative permeance takes the following form in order to take into account the iron core saturation, considering the fundamental harmonic:

$$\Lambda(\alpha) \approx \Lambda_0 + \Lambda_{sat}(\alpha,t) \quad (27)$$

where:

$$\Lambda_{sat}(\alpha,t) = -\Lambda_{sat}\cos\left(2p\alpha - 2\omega_1 t - 2\varphi_s\right) \quad (28)$$

So, the influence of the rotor and stator MMF on the magnetic flux density, due to the saturation will be:

$$b_{sat}(\alpha,t) = \left[F_1(\alpha,t) + F_2(\alpha,t)\right]\Lambda_{sat}(\alpha,t) \quad (29)$$

This means that, in the current spectrum the third harmonic is saturation related.

B. *Presentation of the Proposed Technique*

The skewing has as impact to significantly decrease the amplitudes of the slot harmonics, which produce torque pulsations, noise and losses [2]-[3], resulting to decreased induction motor life-cycle. In the literature, the proposed skewing angle for open rotor slot induction motor is equal to a slot pitch. If the assumption is made that, at the first edge of the motor, opposite from a referenced stator tooth there exists a rotor bar, then along the shaft, at the other motor edge opposite from the same stator tooth there is a rotor tooth. In Fig. 1, one can see the two previously described edges in a 3-phase cage induction motor.

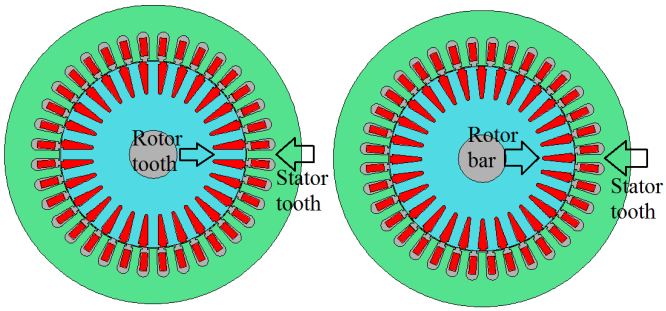

Fig. 1. The two induction motor edges along the shaft, in a skewed cage rotor. Opposite from the referenced stator tooth there is: a) rotor tooth and b) rotor bar.

The aim is to be able to take the skewing into consideration for post-processing calculations, while having simulated a rotating un-skewed induction motor.

Firstly, let's assume as t_0 the moment when spatially the maximum of the rotating magnetic field $B_{\max}$ is located at a stator point (x_0, y_0) on the extension of a bar's bisector. This bar is taken as reference. This happens for all points with the same coordinates (x_0, y_0) along the shaft because the motor is un-skewed.

The magnetic field rotates with $n_s = 60 f_s / p$, while the rotor with $n_{mech} = (1-s) n_s$. At this stage, it is important to identify the exact time $t_{critical}$, at which the magnetic field will reach its maximum at the same point (x_0, y_0) and this point will now be on the extension of any rotor tooth's bisector. This phenomenon happens periodically if n=constant. As a consequence, it is logical to find out the first time that it happens, in order to achieve the minimum value of $t_{critical}$.

The motor has s_2 rotor slots. So, the angle between a bar's and the neighboring rotor tooth's bisectors is $\theta = 180^\circ / s_2$. Moreover, the rotating period of the stator's magnetic field is $T_{sR} = p / f_s$ and the period of the rotor rotation is $T_{mech} = p / \left[(1-s) f_s\right]$.

At the time:

$$t_1 = t_0 + \beta T_{sR}, \beta \in \mathbb{N} \quad (30)$$

one expects to find $B_{\max}$ at the point (x_0, y_0). Naturally, at time:

$$t_2 = t_0 + \gamma T_{mech}, \gamma \in \mathbb{N} \quad (31)$$

the referenced rotor bar's bisector will be at the same position as in t_0.

What matters now is to identify the referenced rotor bar's angular position $\theta(t_1)$ at t_1. Easily, it occurs that:

$$\theta(t_1) = \frac{t_1}{t_2} \cdot 360^\circ \cdot \beta \quad (32)$$

Now, if:

$$\theta(t_1) = 360\gamma \pm \delta\theta, \delta: odd \quad (33)$$

the goal has been achieved. This means that, at this specific time t_1 opposite from the stator point (x_0, y_0), which is characterized by $B_{\max}$, one may find a rotor tooth's bisector, and as a consequence:

$$t_{critical} = t_1 \quad (34)$$

With the use of the FEM simulation, one may calculate several time-dependent variables, like the phase currents and the motor's torque. The extracted signals have been obtained with a specific frequency sampling. This means that, the user has the instant value of the selected variable (current, torque etc) at each specific time. Now, it is needed to phase shift the extracted signal at the calculated $t_{critical}$ and sum it with the original. Then divide the sum by 2. By doing so, the following have been achieved in the occurring signal:

- The stator and rotor MMF related harmonics have been kept intact.
- The geometrical phase difference caused by the skewing is taken into consideration.
- The saturation harmonics have been kept intact.

The main advantage offered by the multi-slice models has been covered with this technique. The user obtains similar results by simulating an un-skewed motor, saving in this way the computational time needed for the other slices. In the next paragraph, the verification of the described method will be shown with 2-D FEM, for a specific induction motor.

III. FEM Simulations

In this paragraph, a 3-phase, 4 pole, 400V, 50Hz, aluminum cast-cage induction motor will be simulated and studied with transient FE analysis. It has 36 stator and 28 rotor slots. The stator winding is delta connected. For all cases, the non-linear

BH magnetic characteristics of the stator and rotor iron cores are taken into consideration.

In order to be realistic, the un-skewed motor will be simulated to operate under nominal load. In this way, the analysis will take into consideration the actual speed oscillations. The load is set 30Nm. The analysis results are presented in Fig. 2.

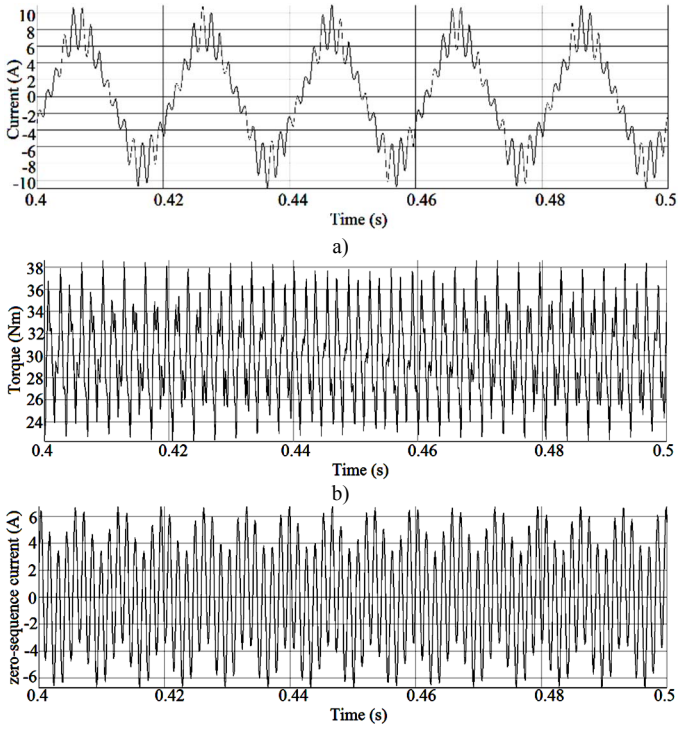

Fig. 2. The electromagnetic variables of the motor under 30Nm operation: a) phase current, b) electromagnetic torque and c) zero-sequence current, versus time.

The speed is now crucial for the proposed technique's application. That's because the speed will determine the phase shifting of the electromagnetic variables. The mean value of the speed is 1465.3rpm. This implies that: $T_{mech} = 0.04094\,\text{sec}$.

After calculations, it occurs that after 7 periods of the magnetic field, the rotor has acquired, with good accuracy, the desired position. This means that the needed phase shifting is 0.28sec. The previously described technique is applied and the new resulting signals are presented in Fig. 3.

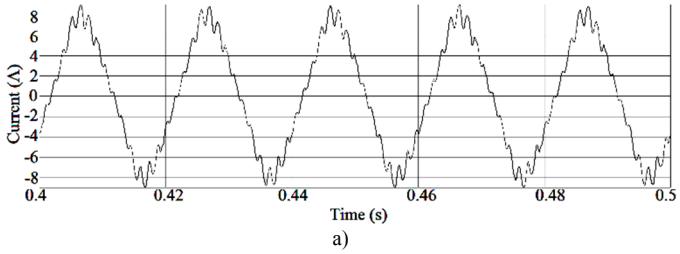

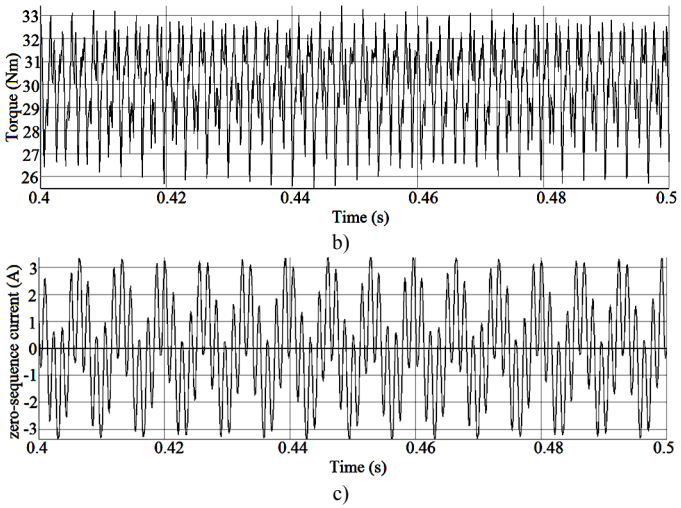

Fig. 3. The transformed electromagnetic variables of the motor under 30Nm operation: a) phase current, b) electromagnetic torque and c) zero-sequence current, versus time.

The comparative phase current spectra of Fig. 2 and Fig. 3 are presented in Fig. 4. The rotor slot related harmonic index (marked with arrows) has been decreased, but still it remains high. The results are due to the fact that, the rotor tooth bisector is not perfectly located on the desired and relative to the magnetic field position. This angle error, is projected through the results in Fig. 4.

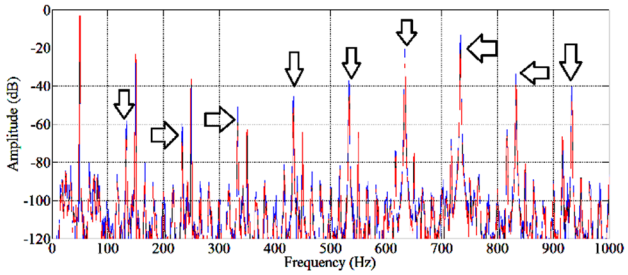

Fig. 4. Comparative spectrums of the phase current for un-skewed motor (blue) and transformed one (red) at frequency area 0-1000Hz, for 30Nm operation.

Since, a little error in the location of the rotor relatively to the magnetic field position strongly affects the harmonic index of the motor, a different strategy should be adopted. Instead of taking as reference the magnetic field period, the rotor will be calculated to be located perfectly at the desired position. The mechanical period of the motor is known. As a consequence, one can calculate the time the rotor needs to take the required position. So considering that $T_{mech} = 0.04094\,\text{sec}$, easily it occurred that $t_{critical} = \frac{360-\theta}{360} T_{mech} \simeq 0.0402\,\text{sec}$.

The un-skewed motor's signals from Fig. 2-a,b,c are phase shifted left at the calculated time $t_{critical}$, then summed with the original ones and divided by 2. The resulting transformed signals are presented in Fig. 5.

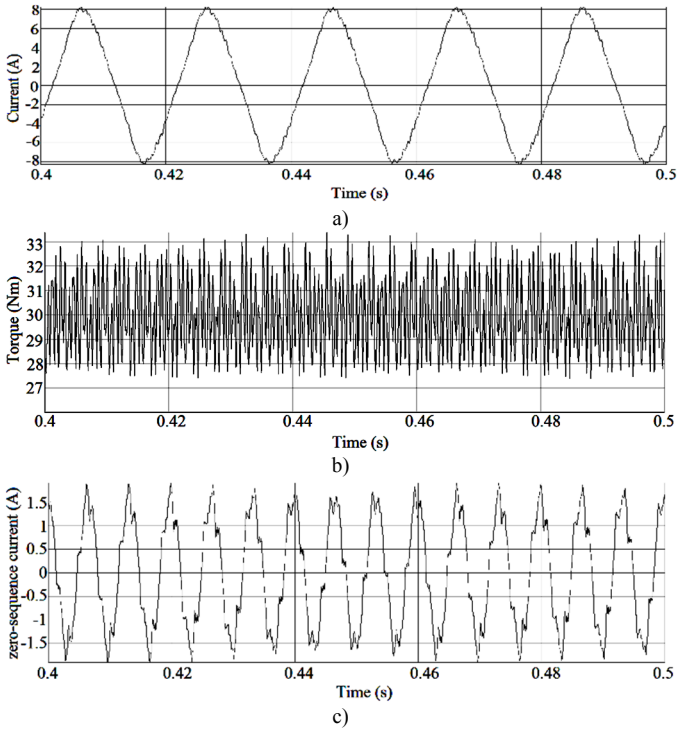

Fig. 5. The second transformation resulting electromagnetic variables of the motor under 30Nm operation: a) phase current, b) electromagnetic torque and c) zero-sequence current, versus time.

The signals presented in Fig. 5, have much less harmonic content than the original ones (Fig. 2). The frequency spectra of the signals Fig. 5-a and Fig. 5-c will be shown in the next paragraph, in comparison to the experimental results.

IV. Experimental Verification

In order to verify the proposed technique, the real motor was tested in the laboratory. The skewing angle has been measured 6.2 degrees, very close to the angle θ, which was previously used for the calculations.

The induction motor was coupled to a DC generator, which has been used as mechanical load. The motor was delta connected and fed by a symmetrical, sinusoidal, 3-phase, 380V system. Using a LABVIEW data acquisition card the motor's currents have been measured and analyzed in MATLAB in order to calculate the signal's FFT. The motor's measured speed is 1465rpm.

In Fig. 6 and Fig. 7, the phase currents and the zero-sequence current are presented respectively in pu values. The rated phase current was 5.3A. This means that the amplitude of the measured phase current is 7.5A, very close to the 8A amplitude which occurred from the simulation (Fig. 5-a).

One can see by comparing Fig. 5-a with Fig. 6 and Fig. 5-c with Fig. 7 that the transformed signals, which occurred from the FEM analysis, match the experimental qualitatively with accuracy. Finally, the phase current amplitude seems to have about 4 times greater amplitude than the zero-sequence current amplitude in both simulation and experimental results.

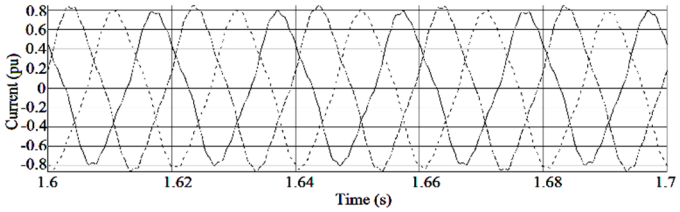

Fig. 6. The induction motor's measured phase currents for speed 1465rpm.

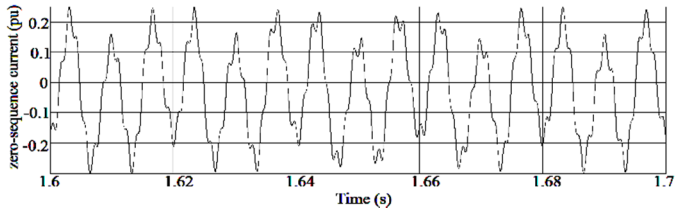

Fig. 7. The induction motor's measured zero-sequence current for speed 1465rpm.

In Fig. 8, the spectra of the transformed simulated and measured phase currents are presented. The locations of the rotor slot related harmonics are marked with arrows. One can see that, the rotor slot related harmonics present decreased amplitudes in the simulated motor's current spectrum, matching with satisfying accuracy the experimental results. The comparison clearly reveals the proposed technique's reliability.

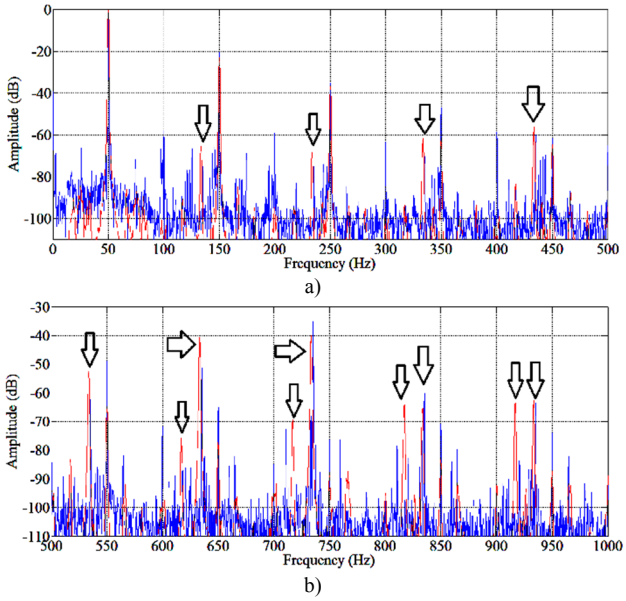

Fig. 8. Frequency spectrum of the transformed simulated phase current (red) and the measured one (blue) for frequency range: a) 0-500Hz and b) 500-1000Hz.

V. Conclusion

In this paper, a new technique for FEM post-processing is presented. With this technique, one can simulate an un-skewed induction motor and transform the time-dependant electromagnetic characteristics in order to include the skewing influence. Analytical calculations have been presented aiming to clearly identify the location of the rotor slot related harmonics in the magnetic field and as a consequence in the current spectrum. The technique has been described thoroughly and tested with 2-D FEM simulations and experimental results.

The methodology described in the paper, is considered a useful tool to the research community, since it presents a clearly great advantage over the multi-slice 2-D models and the 3-D models, concerning the significant reduction of a motor's FEM simulation time.

REFERENCES

[1] E. E. Dreese, "A-C. Elevator Motors of the Squirrel-Cage Type*, "Trans. American Institute of Electrical Engineers,* Vol. 47, No. 4, pp. 1339-1347, Oct. 1928.

[2] L. Prasa and L. Hao, "Interior Permanent Magnet Motors With Reduced Torque Pulsation*, " IEEE Trans. Ind. Electr*., Vol. 55, No. 2, pp. 602-609, Feb. 2008.

[3] H.Y. Yang, Y. C. Lim and H. C. Kim, "Acoustic Noise/Vibration Reduction of a Single-Phase SRM Using Skewed Stator and Rotor*," IEEE Trans. Ind. Electr.*, DOI: 10.1109/TIE.2012.2217715, 2012.

[4] T. D. Nguyen, K.J. Tseng, S. Zhang and H. T. Nguyen, "A Novel Axial Flux Permanent-Magnet Machine for Flywheel Energy Storage System: Design and Analysis*, " IEEE Trans. Ind. Electr*., Vol. 58, No. 9, pp. 3784-3794, Sep. 2011.

[5] K. Kurihara, T. Kubota and M. Hori, "Steady-State and Transient Performance Analysis for a Single-Phase Capacitor-Run Permanent-Magnet Motor With Skewed Rotor Slots, *" IEEE Trans. Ind. Electr*., Vol. 57, No. 1, pp. 44-51, Jan. 2010.

[6] C. I. McClay and S. Williamson, "The Variation of Cage Motor Losses with Skew, *" IEEE Trans. Ind. App*., Vol. 36, No. 6, pp. 1563-1570, Nov-Dec. 2000.

[7] A. Chiba and J. Asama, "Influence of Rotor Skew in Induction Type Bearingless Motor, *" IEEE Trans. Magn*., Vol. 48, No. 11, pp. 4646-4649, Nov. 2012.

[8] A. Boglietti, A. Cavagnino and M. Lazzari, "Computational Algorithms for Induction-Motor Equivalent Circuit Parameter Determination-Part I: Resistances and Leakage Reactances, *" IEEE Trans. Ind. Electr*., Vol. 58, No. 9, pp. 3723-3733, Sep. 2011.

[9] Y. Kawase, T. Yamaguchi, Z. Tu, N. Toida, N. Minoshima and K. Hashimoto, "Effects of Skew Angle of Rotor in Squirrel-Cage Induction Motor on Torque and Loss Characteristics*" IEEE Trans. Magn*., Vol. 45, No. 3, pp. 1700-1703, Mar. 2009.

[10] D. G. Dorrell, P. J. Holik, P. Lombard, H. J. Thougaard and F. Jensen, "A Multisliced Finite-Element Model for Induction Machines Incorporating Interbar Current, *" IEEE Trans. Ind. Appl*., Vol. 45, No. 1, pp. 131-141, Jan/Feb. 2009.

[11] L. Serrano-Iribarnegaray and J. Martinez-Roman, "Critical review of the analytical approaches accounting for interbar currents and experimental study of ageing in two-speed asynchronous motors for elevator drives, *" Proc. Inst. Elect. Eng.-Electr. Power Appl.,* Vol. 152, No. 1, pp. 72-80, Jan. 2005.

[12] R. Carlson, C. A. da Silva, N. Sadowski, Y. Lefevre and M. Lajoie-Mazenc, "The Effect of the Stator-Slot Opening on the Interbar Currents of Skewed Cage Induction Motor, *" IEEE Trans. Magn*., Vol. 38, No. 2, pp. 1285-1288, Feb. 2002.

[13] G. D. Kalokiris, T. D. Kefalas, A. G. Kladas and J. A. Tegopoulos, "Special Air-Gap Element for 2-D FEM Analysis of Electrical Machines Accounting for Rotor Skew, *" IEEE Trans. Magn*., Vol. 41, No. 5, pp. 2020-2023, May 2005.

[14] M. A. Alhamadi and N. Demerdash, "Modeling and experimental verification of the performance of a skew mounted permanent magnet brush-less dc motor drive with parameters computed from 3-D FE magnetic field solutions, *" IEEE Trans. Ener*. Conv., Vol. 9, No. 1, pp. 26-35, Mar. 1994.

[15] S. L. Ho, W. N. Fu and H. C. Wong, "Direct Modeling of the Starting Process of Skewed Rotor Induction Motors Using a Multi-Slice Technique.," IEEE Trans. Ener.Conv., Vol. 14, No. 4, pp. 1253-1258, Dec. 1999.

[16] J. Asama, Y. Hamasaki, T. Oiwa and A. Chiba, "Proposal and Analysis of a Novel Single-Drive Bearingless Motor," *IEEE Trans. Ind. Electr*., Vol. 60, No. 1, pp. 129-138, Jan. 2013.

[17] B. Weilharter, O. Biro, S. Rainer and A. Stermecki, "Computation of Rotating Force Waves in Skewed Induction Machines Using Multi-Slice Models," *IEEE Trans. Magn*., Vol. 47, No. 5, pp. 1046-1049, May 2011.

[18] D. Torregrossa, B. Fahimi, F. Peyraut and A. Miraoui, "Fast Computation of Electromagnetic Vibrations in Electrical Machines via Field Reconstruction Method and Knowledge of Mechanical Impulse Response," *IEEE Trans. Ind. Electr*., Vol. 59, No. 2, pp. 839-847, Feb. 2012.

[19] OPERA-2D Reference Manual, Version 14R1, Vector Fields Software, Cobham Technical Services, pp.390, Jul. 2011.

[20] J. J. C. Gyselinck, L. Vandelde and J. A. A. Melkebeek, "Multi-Slice FE Modeling of Electrical Machines With Skewed Slots-The Skew Discretization Error," IEEE Trans. Magn., Vol. 37, No. 5, pp. 3233-3237, Sep. 2001.

[21] K. N. Gyftakis, D. V. Spyropoulos, J. Kappatou and E. D. Mitronikas, "A Novel Approach for Broken Bar Fault Diagnosis in Induction Motors through Torque Monitoring," *IEEE Trans. Energy Conv.*, DOI: 10.1109/TEC.2013.2240683, 2013.

[22] K.N. Gyftakis and J.C.Kappatou, " A Novel and Effective Method of Static Eccentricity Diagnosis in 3-Phase, PSH-Induction Motors*," IEEE Trans. Ener. Conv.*, DOI: 10.1109/TEC.2013.2246867, 2013.

[23] B. M. Ebrahimi, J. Faiz, M. J. Roshtkhari, "Static-, Dynamic-, and Mixed-Eccentricity Fault Diagnoses in Permanent-Magnet Synchronous Motors*", IEEE Trans. Ind. Electr*., Vol. 56, No.11, pp. 4727-4739, Nov. 2009.

[24] P. Zhang, Y. Du, T. G. Habetler and B. Lu, "A Survey of Condition Monitoring and Protection Methods for Medium-Voltage Induction Motors*", IEEE Trans. Ind. Appl*., Vol. 47, No.1, pp. 34-46, Jan/Feb 2011.

[25] J. F. Gierras, C. Wang, and J. C. Lai, Noise of Polyphase Electric Motors, CRC Press, pp. 39-43, 2006.